MERIS Cloud Albedo and Cloud Optical Thickness

Algorithm Theoretical Basis Document

ATBD 2.1 & ATBD 2.2

Jürgen Fischer, Rene Preusker, Lothar Schiller

Free University Berlin
Institute for Space Science

Contents

1   Introduction

Clouds have a strong modulating influence on the global energy budget. There is a general agreement that the annual global mean effect of clouds is to cool the climate system, but there is a significant disagreement on the magnitude, which exceeds 10 W/m^2 (Arking, 1990). To improve such estimates, the cloud cover fraction, cloud type and the cloud top height have to be known more accurately.

The most important cloud parameter for energy budget studies is the cloud albedo. Even small changes in the cloud albedo affect significantly the earth climate. In general, variations in cloud cover may cause both, cooling or heating effects, because the shortwave as well as the infrared flux is affected. In contrast, the enhancement of albedo alone does not affect the infrared radiation but the reflection of more solar radiation leads to cooling effects. The cloud albedo depends on the cloud optical thickness and this varies with the liquid water content and size distribution of the cloud droplets. An increase in the number of cloud droplets, e.g. due to an increase in aerosol concentration, results in a decreased mean droplet size, for constant liquid water content. This increases the cloud albedo and may reduce the greenhouse effect of the trace gases. There are considerable uncertainties in the understanding of the process leading from artificial and natural emission of SO_2 to cloud optical properties, which may compensate the warming effect of CO_2 and other trace gases (Charlson *et al*., 1987). These effects can be responsible for an increase of 10% in reflected radiation, if clean maritime air is replaced by continental like aerosol characteristics in general circulation models (Twomey, 1977).

The cloud optical thickness is also an important parameter for the surface and atmospheric energy budget. The variation of cloud optical thickness alters the amount of reflected radiation and hence the energy that reaches the surface. Investigations based on general circulation models show, that an increase in optical thickness and water/ice content of clouds may results in a negative temperature feedback. This opposes the positive feedback due to cloud cover changes (Roeckner, 1987).

Satellite observations are the most effective method to observe clouds on a large scale and to estimate their impact on the earth's climate. Therefore longterm satellite observations are necessary to enable the retrieval of variations in cloud optical properties. For example, the International Satellite Cloud Climatology Project (ISCCP) collects and analyses satellite radiance measurements to infer the global distribution of cloud radiative properties and their diurnal and seasonal variations (Rossow, 1989). The cloud optical thickness can be determined directly from reflectance data, if the particle size is known. Rossow and Lacis (1988) assumed for ISCCP analysis, that all clouds can be interpreted as having an effective radius of $re=10\mu m$. A more accurate estimation of optical thickness can be made if the particle size and phase are included in the algorithm development.

Twomey and Seton (1980) described in a theoretical study the potential of simultaneous measurements of the optical thickness and mean radius if using near infrared radiances. Nakajima and King (1990) showed that measurements of reflectances at $0.75\mu m$ and $2.16\mu m$ can be used to estimate for optical thickness and effective radius. As there is no infrared channel for the MERIS instrument the radiance at $O=753.75nm$ (channel 10) with a spectral width of 7.5nm is related to the optical thickness and cloud albedo by considering the observation geometry. The measurements in this channel are free of a considerable influence of atmospheric absorption due to gases or liquid water.

This document provides a description of the MERIS algorithms for the retrieval of cloud optical thickness and cloud albedo. The principle approach is the use of a large dataset of radiative transfer simulations covering the whole range of possible observation conditions (viewing- and sun zenith angles) as well as radiative and geometric properties of clouds and aerosols. A polynomial regression has been used for the inversion of the dataset in order to derive the desired cloud parameter from MERIS radiance

measurements.

For a validation of the global retrieval of cloud optical thickness and albedo, aircraft measurements with multispectral radiometers and cloud microphysical instruments build a basis of evaluating the performance and accuracy of the proposed algorithms.

2   Algorithm Overview

The cloud albedo α_c and cloud optical thickness δ_c will be estimated from measurements of the MERIS channel centred at λ=753.75nm. An adequate algorithm is established to transform the radiance measurements into hemispherical quantities by integration over viewing angles, since clouds do not reflect the sunlight isotropic. The algorithm accounts for the angular distribution of reflected solar radiation by means of radiative transfer simulations. The radiative transfer model MOMO (Matrix Operator Model) is used to solve the forward problem and simulates the satellite sensor signals (radiances), considering the relevant radiative transfer processes in the atmosphere. MOMO calculates the spectral albedo at the atmospheric model layer boundaries.

Inferring the optical properties from measured satellite radiances is called the inverse problem. This problem will be tackled by a polynomial approach where the cloud albedo and optical thickness are related to a polynomial function of the radiance to be measured. In order to improve the algorithm, the selection of the coefficients for polynomials depends on parameters that are specified *a priori*, either from external data or empirically derived from climatological data sets. The surface albedo as the most important parameter is taken from the MERIS AlbedoMap data set, a global, temporally resolved data base of surface albedo (Muller et al., 2006). It provides global 16-day averages of surface reflectance in the MERIS window channels on a rectangular longitude-latitude grid at a spatial resolution of 0.05°.

3   Algorithm Description

3.1   Theoretical Description

3.1.1   Physics of the Problem

3.1.1.1 Cloud Albedo

Satellite instruments usually measure directional intensity quantities, which have to be converted into fluxes for an albedo retrieval. The radiation field above a cloud layer is non-isotropic (see Figure 1), because of the strong angular dependency of a single-scattering process, expressed by the scattering phase function of cloud particles. The inference from radiance measurements to albedo requires the knowledge of the solar zenith angle and the viewing geometry.

The spectral albedo of a surface (in our case: cloud top level) is defined as the ratio of radiant flux $\Phi^\uparrow$, which is directed to the upper hemisphere to the incident radiant flux $\Phi^\downarrow$:
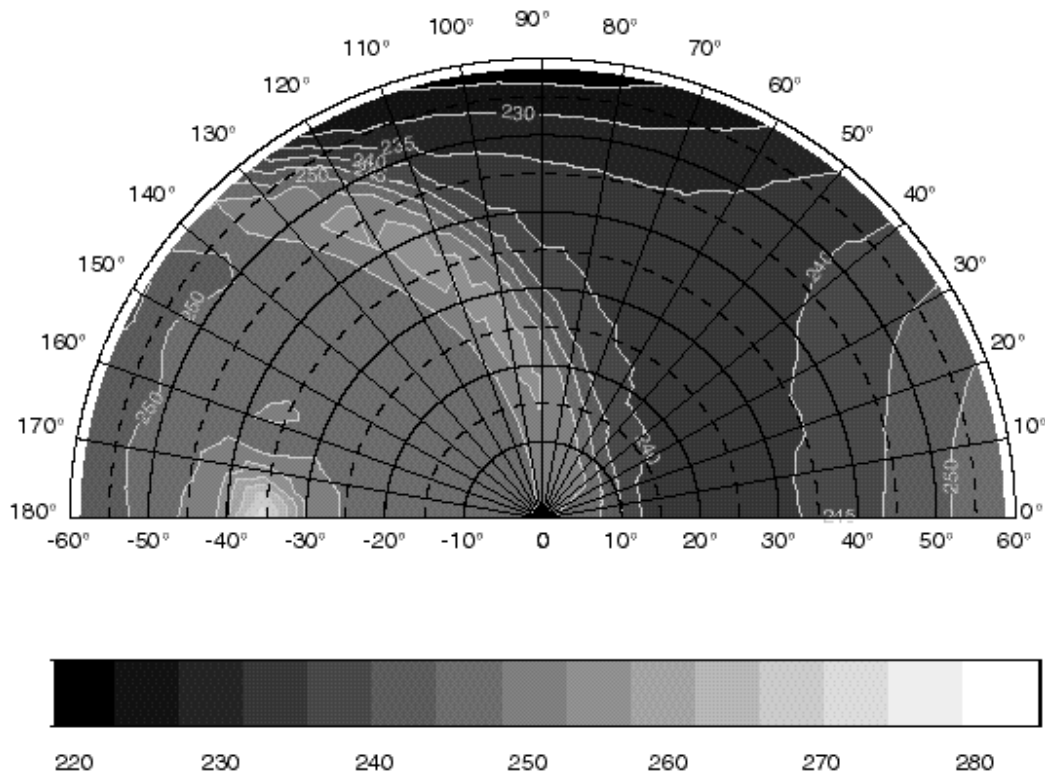

Figure 1: *Non-isotropic radiance field as simulated with the radiative transfer code MOMO. Polar-plot of upward directed radiances at the top of the atmosphere. The sun zenith angle is 35 degrees. Cloud parameters: optical thickness $\delta_c=30$, cloud geometrical thickness: 2km, cloud top height: $z_{top}=2.5km$, effective radius: $r_e=17\mu m$. Calculations for MERIS channel 10 ($\lambda=753.75nm$).*
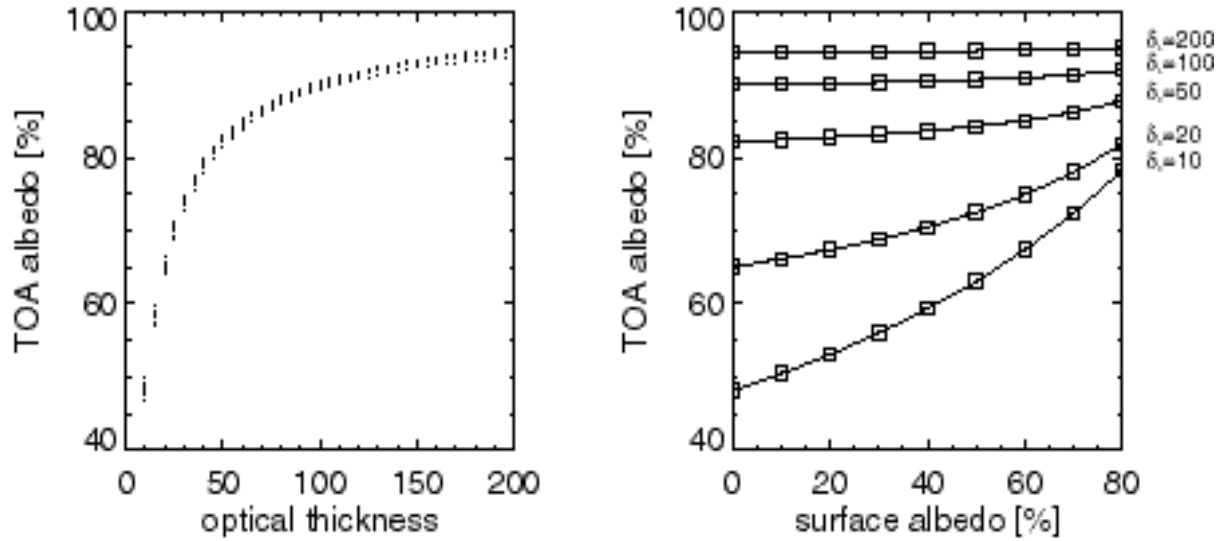
Figure 2: *Left: Cloud albedo (at top of atmosphere TOA) as a function of cloud optical thickness (MOMO simulations) for all cloud droplet size distributions used for the inversion process. (sun zenith angle 35°) Right: Cloud albedo as a function of surface albedo (MOMO simulations). The influence of surface reflection is shown for clouds with various optical thicknesses.*

$$\alpha_\lambda(\vartheta_s) = \frac{\Phi_\lambda^\uparrow(\vartheta_s)}{\Phi_\lambda^\downarrow(\vartheta_s)}. \qquad (1)$$

The hemispherical fluxes are derived with the simulated radiance values by integration over the hemisphere:

$$\Phi_\lambda(\vartheta_s) = \int\int L_\lambda(\vartheta_v, \vartheta_s, \varphi) d\vartheta_v d\varphi. \qquad (2)$$

The downward flux at cloud top level depends on the amount of solar irradiation F_0 and is a function of the sun zenith angle ϑ_s. The modification of the downward flux due to aerosols and absorption by atmospheric gases is usually small at λ=753.75nm and can be neglected. The upwelling flux above clouds depends on the droplet size and liquid water content of the cloud. Usually these parameters have a distinct vertical profile within the cloud.

In Figure 2, the cloud albedo is shown as a function of optical thickness (left). For optically thin clouds, a small increase in cloud optical thickness leads to a strong enhancement of cloud reflectivity, in contrast to optically thick clouds, where cloud albedo modification due to changes in optical thickness is rather small, but might be important with respect to the impact on climate. This relation between cloud albedo and optical thickness is slightly affected by different droplet sizes as shown in the left graph of Figure 2.

Most of the broadband measurements of existing satellite instruments are affected by water vapour and/or the absorption by the liquid water in the cloud droplet itself. In contrast, the narrow-band MERIS channel 10 used for the estimation of the cloud albedo, is not affected by absorption. Therefore, the

spectrally integrated broadband albedo derived from broadband measurements is expected to be lower than cloud albedo derived from narrow-band measurements in window channels.

Since the surface reflection affects the up-welling radiation even under thick clouds, the surface albedo has to be considered for the evaluation scheme. The influence of surface albedo and cloud albedo is shown in Figure 2 (right).

3.1.1.2 *Cloud optical thickness*

In addition to the effective radius, the optical thickness of a cloud is the most important parameter to describe cloud shortwave radiative properties. A formal definition uses the extinction efficiency factor Q_e:

$$\delta_c = \int_0^z \int_0^\infty n(r) Q_e \pi\, r^2 dr\, dz \approx 2\pi \cdot \int_0^z \int_0^\infty n(r) r^2 dr\; dz \;.$$ (3)

The extinction efficiency depends on droplet radius r, wavelength λ and refractive index of water or ice m and is defined as the ratio of the extinction to the cross-sectional areas of droplets. Under the assumption of spherical particles, it can be derived by Mie theory. The size spectrum of the cloud particles is denoted with $n(r)$ and z is the vertical coordinate. Q_e tends to become a constant value of 2, if the ratio of particle radius to wavelength is large (*i.e.* for solar radiation in the visible and near infrared as well as for typical cloud droplet size distributions). In that case, δ_c is a function of droplet size distribution and total number of cloud droplets (right hand side of Equation 3). The effective radius of a size distribution is defined by (Hansen and Travis, 1974):

$$r_e = \frac{\int_0^\infty r^3 n(r) dr}{\int_0^\infty r^2 n(r) dr}\;.$$ (4)

The values for the effective radius vary usually between $r_e = 4\mu$m and $r_e = 30\mu$m. A simple relation between the effective radius, the liquid water path (LWP) and the optical thickness is given by Stephens (1978):

$$\delta_c \approx \frac{3}{2} \frac{LWP}{r_e}\;.$$ (5)

The lack of information about the effective radius limits the accuracy of cloud optical thickness retrieval. Additionally, the increase of radiance with optical thickness has a tendency for saturation at higher values (Figure 2), thus, the determination of high values of cloud optical thickness is very sensitive to uncertainties in the measurement and in the retrieval algorithm (Figure 10).
The reflection of the underlying surface affects the upwelling radiation even under a thick cloud. Therefore, surface albedo is introduced into the evaluation scheme for both parameters.

3.1.2 Mathematical Description of the Algorithm

3.1.2.1 Radiative Transfer Calculations

Radiative transfer simulations have been performed to create a data set as a basis for the inversion process. They should cover the whole range of possible conditions and account for all parameters and processes, affecting the retrieval.

The radiative transfer model MOMO (Fischer and Graßl, 1991; Fell and Fischer, 1995) uses optical properties of a cloud droplet ensemble as calculated from a Mie-program (Wiscombe, 1980). For a given droplet size distribution and optical constants of water and ice (complex refractive indices from Hale and Querry (1973), Palmer and Williams (1975) and Irvine and Pollack (1968)) the Mie-code returns extinction and scattering coefficients and the scattering phase function, which describes the angular distribution of scattered light in a single scattering event. The droplet size distribution is approximated by an analytical function (modified gamma distribution):

Table 1: Cloud types used in the radiative transfer simulations with the ranges of the properties.

No.	cloud type	effective radius (µm)	extinction (km^{-1})	cloud optical thickness
1	stratus I	17	15-20	2-8
2	stratus II	10	15-20	2-8
3	stratocumulus I	17	16-24	2-14
4	stratocumulus II	10	16-24	2-14
5	nimbostratus	17	20-30	100-250
6	altostratus	8	15-20	8-22
7	cumulus	25	15-20	8-22
8	cumulonimbus	33	25-35	150-350
9	altocumulus	8	16-24	8-22
10	stratus + altostratus I	-	16-24	20-100
11	stratus + altostratus II	-	15-20	20-100

$$n(r) = r^{\frac{1-3r_b}{r_b}} \cdot e^{\frac{-r}{r_e \cdot r_b}}, \tag{6}$$

which is determined by two parameters: the effective radius r_e and a dispersion r_b about the effective radius.

The scattering coefficient for λ=753.75nm is an input parameter of the radiative transfer model MOMO. In contrast, the scattering phase function has to be expanded into a Fourier series in order to calculate azimuthally resolved radiances. Since MOMO calculations include the full information on the angular dependencies of scattering due to cloud particles, radiance measurements can be simulated for any illumination and observation geometry as well as for any atmospheric conditions. Several viewing conditions have to be simulated for each cloud case. Due to the Matrix-Operator-assumption of MOMO, the discrete zenith angles are not equidistant. The discrete azimuth angles are equidistant; 17 values has been selected between 0° and 180°. Since the simulated radiation field is symmetric to the sun-pixel-

sensor-plane, only the angles in this interval have to be considered. For the determination of MERIS signals in the 753.75nm band (7.5nm bandwidth) the band averaged values are used.

Cloud optical thickness varies between 1 and 350 in the calculations. Figure 3 shows the number distribution of considered optical thicknesses (see Table 1).

The range of the used surface albedos contains values from 0% to 80% in steps of 10%. Due to the multi-scattering processes within cloud layers and a more or less isotropic irradiation at the earth surface, the assumption of an isotropic reflection at the earth's surface is sufficient for the algorithm development.
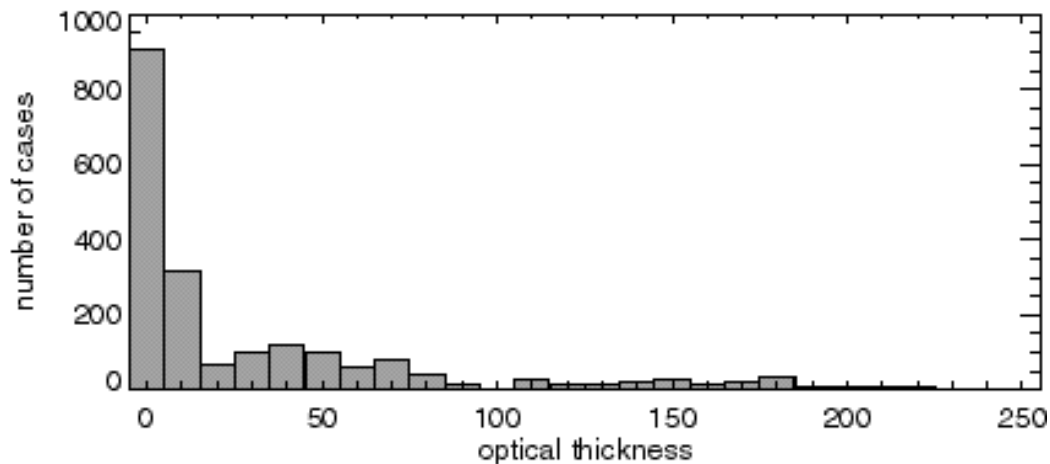

Figure 3: *Statistical distribution of the cloud optical thickness values considered in the radiative transfer simulations.*

Since the cloud top height slightly affects the radiance at top of atmosphere, four different cloud top heights are used. For cloud optical thicknesses $\delta_c > 10$ the influence of the aerosol scattering is almost negligible for its retrieval. For optically thin clouds aerosols modify the intensity and anisotropy of the backscattered radiation. Therefore two standard aerosol models, *maritime* and *continental*, with an optical thickness of $\delta_{aero}=0.125$ at $\lambda=550$nm according to Toon and Pollack (1973) are applied in all simulations.

Since it is not possible to perform radiative transfer calculations for all permutations of input parameters, a limit of 2000 radiative transfer simulations were performed, which might represent typical variations of cloud type ($\cong$ effective radius), optical thickness, aerosol type and surface albedo. The cloud types used in the radiative transfer simulations as well as their range of optical properties are listed in Table 1.

In case of volcanic eruptions stratospheric aerosols should be introduced in the model atmosphere. Sulphuric acid particles are then placed in the model layer between 20km and 30km (WCP-report No. 112, 1986). The influence of volcanic ashes does not seem to be important for our purposes, because they tend to modify the signals in the region of the eruption only.
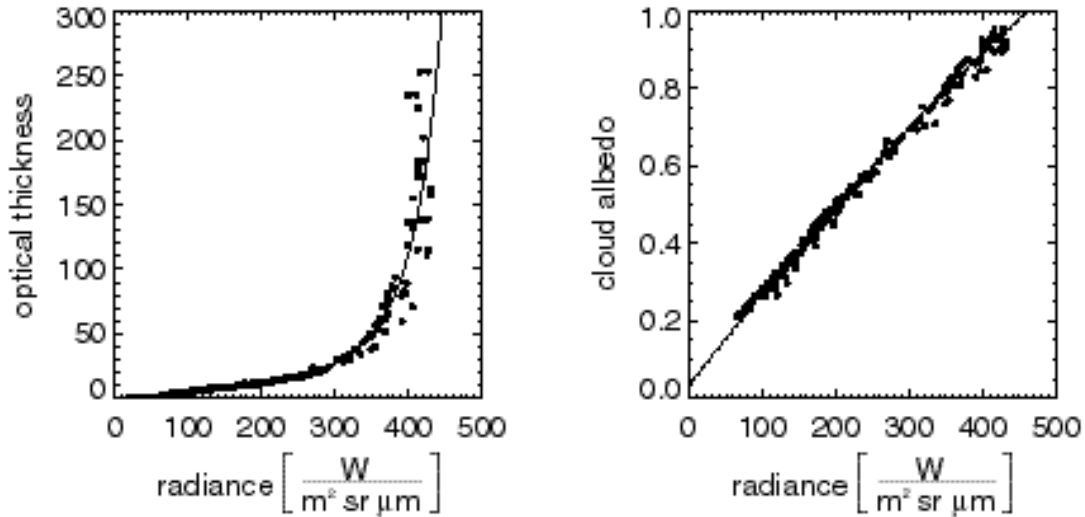
Figure 4: *Simulation results (circles) and regression functions (solid lines) for the cloud albedo retrieval (left) and the cloud optical thickness retrieval (right). Solar zenith angle $\vartheta_0=35°$, viewing zenith angle $\vartheta_v=0°$ and azimuth difference $\Delta\phi=0°$. A surface albedo of 40% was assumed for this example. Regression coefficients: r=0.9991, $\chi^2=0.007$ (cloud albedo) and r=0.997, $\chi^2=0.101$ (logarithm of cloud optical thickness).*

3.1.2.2 Polynomial Approach

The impact of the cloud properties on the radiance measurements can be described by a polynomial expression. Here the cloud albedo and the cloud optical thickness are related to the radiance value in the MERIS channel 10 at λ=753.75nm ($\Delta\lambda$=7.5nm), whereby the coefficients are determined from radiative transfer calculations.

A second order polynomial fits the functional dependence between cloud albedo and radiance with an acceptable accuracy:

$$\alpha_{cl} = a_0 + a_1 \cdot L + a_2 \cdot L^2 . \qquad (7)$$

For the cloud optical thickness, the following relation has been used to approximate the simulated data:

$$\delta_c = \exp(b_0 + b_1 \cdot L + b_2 \cdot L^2 + b_3 \cdot L^3) \qquad (8)$$

Two types of parameters have to be distinguished: parameters known or estimated *a priori* (solar and viewing geometry, surface albedo, aerosol type according to land/sea pixel identification, thermodynamic phase) and unknown parameters, which have to be regarded as sources of noise such as effective radius.

The polynomial coefficients have to be specified for all observation and sun geometry- and observation parameters that are known *a priori*. For each specific case, determined by the set of *a priori* known parameters, a multi-linear regression method has been applied to find the appropriate coefficients. The resulting regression coefficient *r* can be used for an error estimation.

3.1.2.3 Inversion

Figure 5 describes the inversion process. The radiance is processed with the coefficients in a polynomial evaluation. Additional data such as surface albedo will be used for a pre-selection to find the appropriate coefficients. The coefficients are related to the discrete MOMO angles and have to be interpolated to the actual observation and solar geometry as well as to the surface albedo of the pixel.

A stratospheric aerosol flag is set, if volcanic eruptions with emissions in the stratosphere are reported. In such cases the algorithm selects the coefficients (or matrices) derived with the simulations containing sulphuric acid particles in the upper atmosphere.
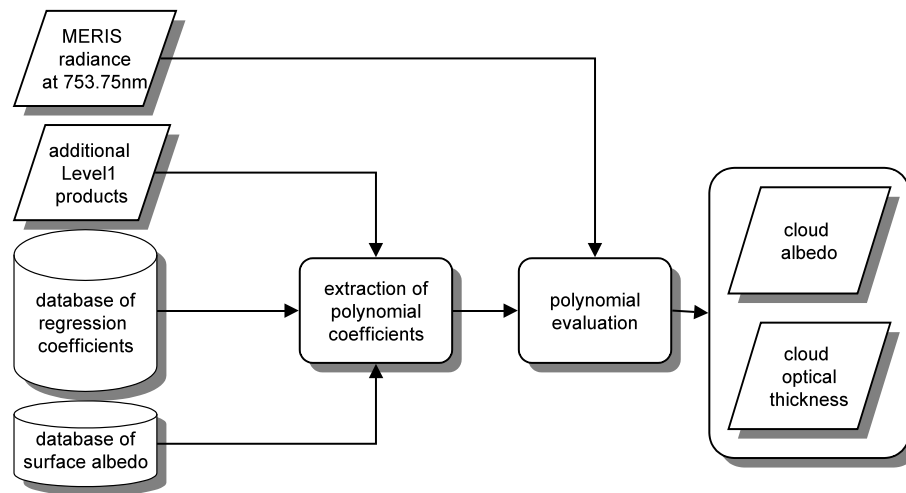

Figure 5*: Flowchart diagram of the inversion process of the cloud albedo and cloud optical thickness retrieval.*

3.2   Practical Considerations

3.2.1   Numerical computation considerations

The size of the coefficient database for a polynomial approach could be estimated from the number of different surface albedo values and angular resolution of MOMO. Coefficients sets should be available for each surface albedo and stratospheric aerosol flag status.

3.2.2 Calibration and Validation

For a calibration and validation of the cloud optical thickness and cloud albedo retrieval, field campaigns including aircraft observations as well as further radiative transfer calculations are requested. Simultaneous measurements of the size distribution of cloud droplets, their vertical profile within clouds and radiance measurements above clouds as performed, *e.g*. during the CLOUDYCOLUMN campaign as a part of the second Aerosol Characterisation Experiment ACE 2 (Raes, 1997), provide more insight in cloud-radiation-processes and validation opportunities.

Figure 6 shows the cloud optical thickness retrieved from measurements of the upward directed radiance at 753.75nm with the airborne spectrometer OVID (Schüller and Fischer, 1997). The MERIS algorithm as described in this documents has been applied to the measurements and the results agree well with the cloud optical thicknesses, calculated from the vertical distribution of droplet concentration, droplet size and liquid water content measured with *in situ* instruments (Brenguier *et al*., 1999).

A validation of the radiative transfer MOMO has been carried out with measurements (Fischer *et al*., 1991) as well as with other radiative transfer simulations for which good agreements are found (Heinemann and Gentili, 1995; Fell and Fischer, 1995; Santer et al, 2005).
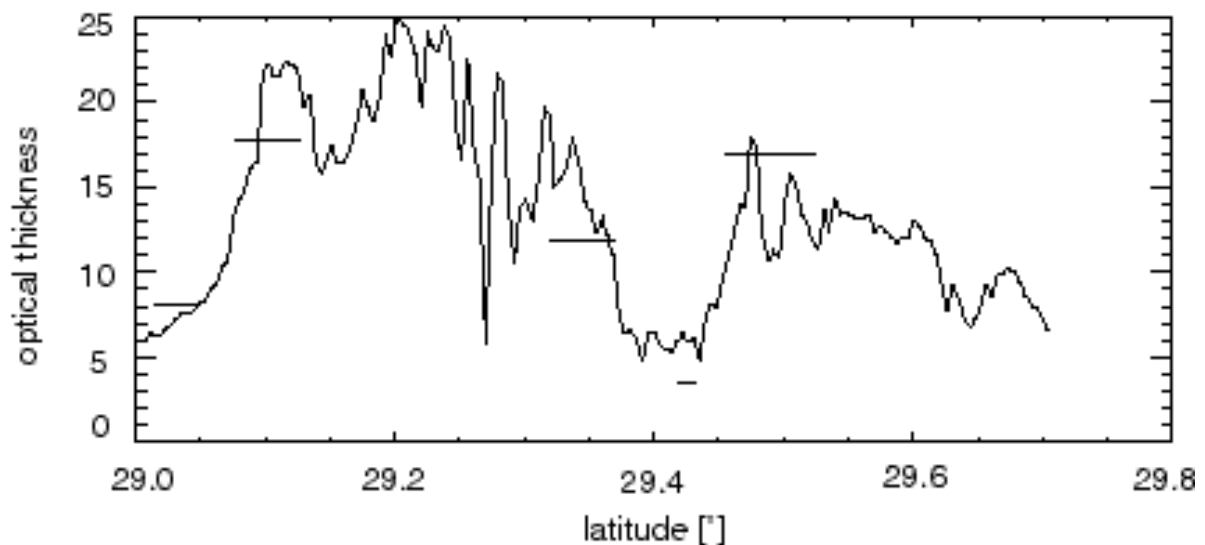

Figure 6: *Comparison of the remotely sensed optical thickness with OVID data (solid lines) with the estimations from in-situ measurements (thick segments) for one leg ACE 2 mission at 26th July 1997 (Brenguier et al., 1999).*

3.2.3 Quality Control and Diagnostics

A diagnostic and a quality control of the estimated cloud albedo are difficult to achieve. The variability, minima and maxima in relation to the observed clouds could be applied. Comparison to cloud properties derived from other satellite instruments might also be used.

3.2.4 Exception Handling

The algorithm will be applied only for pixels that are indicated as cloudy by the cloud-screening algorithm. Pixels for which the quality test (previous section) failed will pass the algorithm without a result. If the algorithm retrieves parameters, which lie outside realistic values, a quality flag will be raised, indicating, which parameter is outside the considered limit. For that specific pixel, no cloud parameter will be estimated.

3.2.5 Output Product

The output of the algorithm are
* cloud albedo
* cloud optical thickness

3.3 Estimates of accuracy and sensitivity

The influence of the regression on the accuracy of the retrieved product is shown in Figure 7 for cloud optical thickness and for cloud albedo as a function of solar zenith angle and viewing zenith angle. Both graphs show that the retrieval of cloud optical thickness as well as the retrieval of cloud albedo is more difficult for larger solar zenith angles. The Figure shows clearly the higher sensitivity of the cloud optical thickness retrieval on solar zenith angle compared to the cloud albedo retrieval.
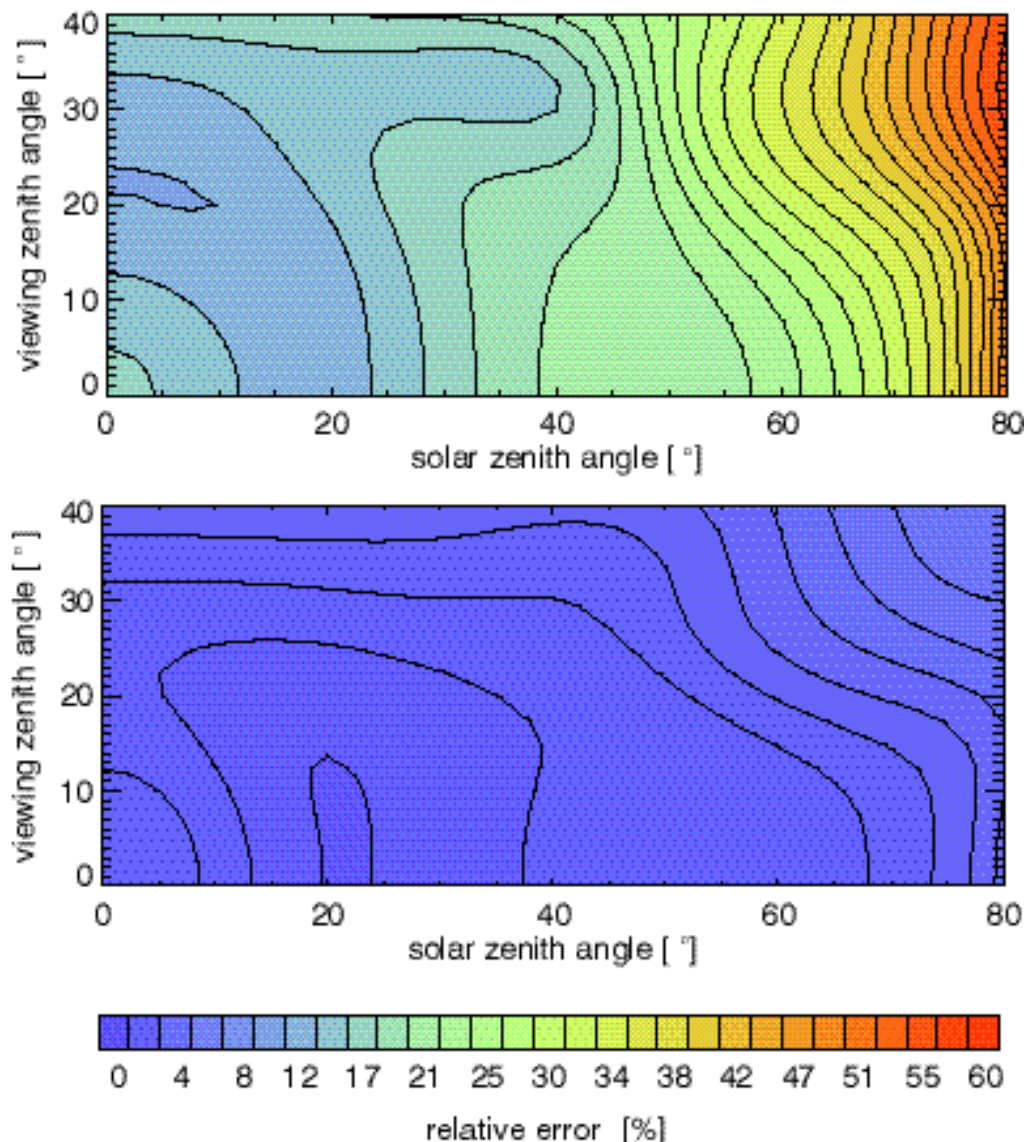

Figure 7: Relative error in percent in retrieved cloud optical thickness (upper graph) and cloud albedo (lower graph) due to regression errors as a function of viewing zenith angle ϑ_v and solar zenith angle ϑ_s (azimuthal difference $\Delta\phi = 90°$, surface albedo $\alpha_s = 0\%$).

This study is focused on a sensitivity analysis, which considers the influence of the observation geometry within a representative MERIS swath, the instrumental noise as well as other atmospheric and surface properties on the accuracy of the retrieved cloud product. Since a complete sensitivity study would

require a systematic and independent variation of all these parameters, which is quite difficult to achieve, we reduced the number of combinations by limiting the range of parameters to values as they occur during the overpass of a representative MERIS swath.

Two steps are performed to access the quality of the algorithm. Firstly, the radiance values for each pixel of the swath have been computed as a function of the parameter under investigation, by using radiative transfer simulations of MERIS Channel 10 and 11. In a second step, we applied the MERIS cloud albedo, cloud optical thickness and cloud top pressure algorithms to these pseudo MERIS images. Beside the images, swath averages of retrieved values, deviations and relative errors are produced in order to quantify the overall effect of these parameters. Projections of the swath images to a map should help to identify geographic regions, where the retrieval is critical (e. g. high solar zenith angles at high latitudes).

3.3.1 Simulation of MERIS images

The properties of the considered MERIS swath simulation are listed in Table 2. This particular swath has been selected, because it covers areas over ocean (70% of all pixels) and land surfaces of different reflectivity (30 % of all pixels), which is quite representative for the land-ocean coverage fraction of the whole earth. The orbital parameter of ENVISAT and the viewing geometry of the MERIS sensor have been used to calculate longitude and latitude as well as the solar and viewing zenith angle and the azimuth difference of each pixel.

The land surface albedo is taken from the data-set of the *International Satellite Land Surface Climatology Project* ISLSCP (Sellers *et al*. 1995). The surface albedo is an integrated value over the entire solar spectrum, thus no wavelength dependencies are considered. Because of the very large solar zenith angles in the northern and southern part of the swath where an estimate of cloud top pressure, cloud optical thickness and cloud albedo is not possible, we restricted our analysis to the range between 70° N and 55° S latitude.

Table 2*: Properties of the considered MERIS swath.*

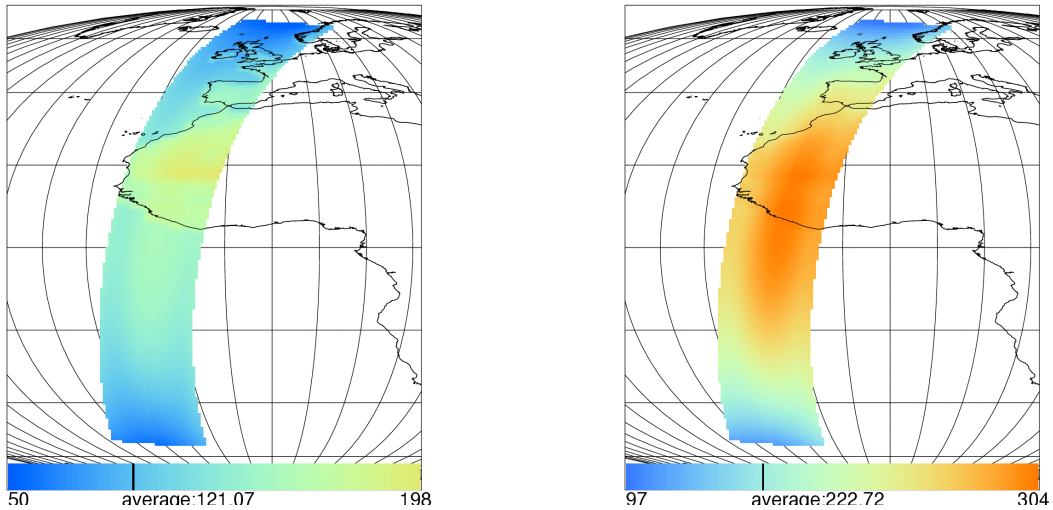|	
Day of the year	80
Measuring time	1100 sec
Satellite inclination	1.72°
Satellite altitude	799 km
Equator crossing time	10:00
Latitude range	70°N – 55°S
Longitude range	15°E – 29°W
Solar zenith angle range	26° - 71°
Viewing zenith angle range	0° - 40°
Azimuth difference range	0° - 180°
Surface albedo range	0% - 40%

Figure 8: Simulated MERIS swath for radiances at channel 10 (753.75nm) calculated with a cloud optical thickness of $\delta_c = 10$ (left) and $\delta_c = 50$ (right).

3.3.2   Cloud optical thickness

3.3.2.1 Sensitivity to geometry

Retrieved cloud optical thickness along a MERIS swath is shown in Figure 9. The optical thickness, assumed for the radiative transfer simulations, is constant for the entire swath. Even for $\delta_c = 10$ (left) the surface structure nearly disappears. The algorithm seems to under-estimates the optical thickness for observation geometries, which are closer to the edge of the swath.
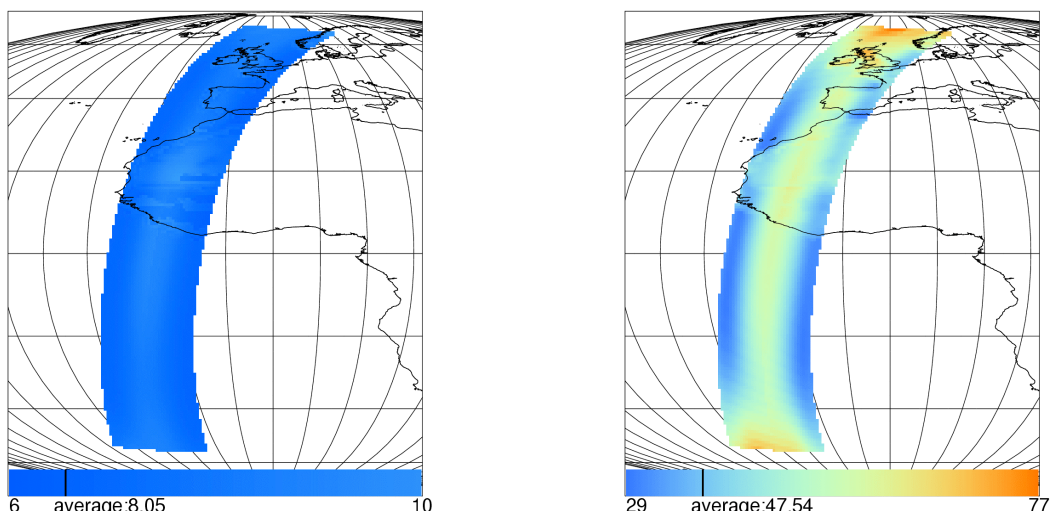

Figure 9: Retrieved cloud optical thickness from simulated MERIS measurements calculated with a cloud optical thickness of $\delta_c = 10$ (left) and $\delta_c = 50$ (right).

At higher latitudes the optical thickness is overestimated. For this MERIS swath averages of δ_c(swath-average) = 8.05 (left) and δ_c(swath-average) = 47.54 (right) have been retrieved.

3.3.2.2 Sensitivity to cloud optical thickness and cloud top height

The sensitivity to cloud optical thickness and cloud top height variations has been analysed with the general finding, that the RMSE (root mean square error) increases with optical thickness. For typical values of δ_c=50 a RMSE=9 has been estimated. The influence of the cloud top height is obvious with a general tendency to higher RMSE values for higher cloud top heights. The root mean square error RMSE (upper graph) and BIAS (lower graph) is shown in Figure 10. The BIAS drastically increases with cloud top heights. Optically thick and low clouds are underestimated with respect to the optical thickness.
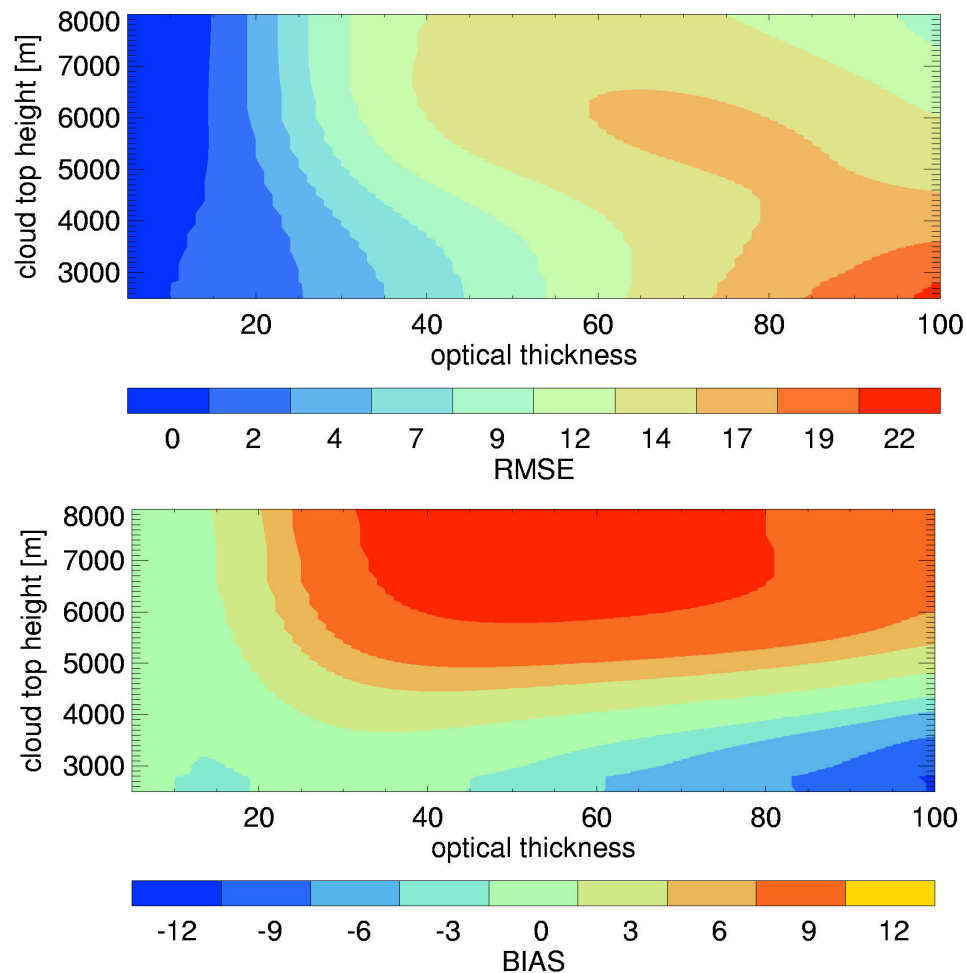

Figure 10: *Sensitivity of the cloud optical thickness retrieval to cloud optical thickness and cloud top height. Root mean square error RMSE (upper graph) and BIAS (lower graph).*

3.3.2.3 Sensitivity of cloud optical thickness retrieval to surface albedo

The sensitivity of the cloud optical thickness retrieval to the surface albedo is shown in Figure 11. The root mean square error RMSE (upper graph) is lower at high and low surface albedo values when the optical thickness is smaller than 50. The largest errors occur at surface albedos of 50% and high optical thickness. These results have to be interpreted with respect to the algorithm development, which is driven by the minimisation of the overall errors.

The lower graph of Figure 11 is showing the BIAS of the retrieved optical thickness. The lowest values for the BIAS are found for optical thicknesses of $\delta_c \sim 50$.
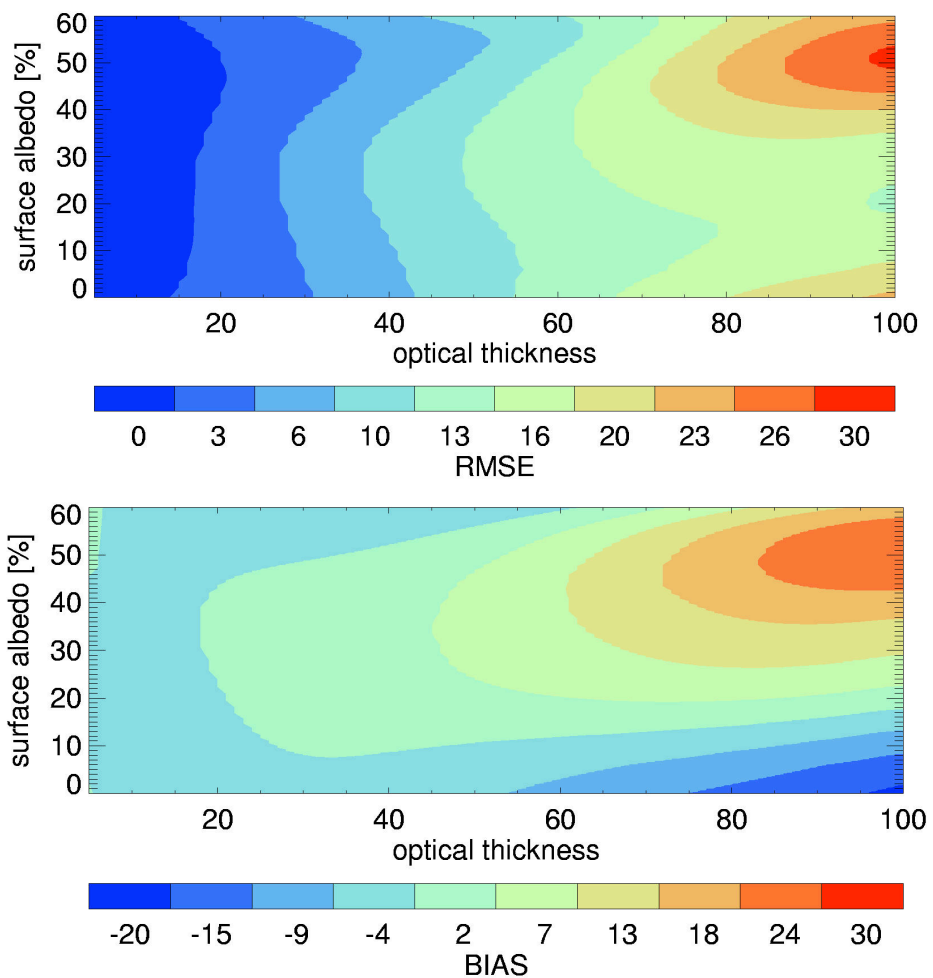

Figure 11: Sensitivity of the cloud optical thickness retrieval to cloud optical thickness and surface albedo. Root mean square error RMSE (upper graph) and BIAS (lower graph).

3.3.2.4 Sensitivity to cloud optical thickness and instrumental noise

Figure 12 shows the sensitivity of the cloud optical thickness retrieval to cloud optical thickness and instrumental noise. The sensitivity of cloud optical thickness to instrumental noise is low compared to the sensitivity to other parameters. Within the considered range RMSE values between 0.03 and 0.07 % are found. The BIAS is more important and reaches values up to $\delta_c \sim -12$.
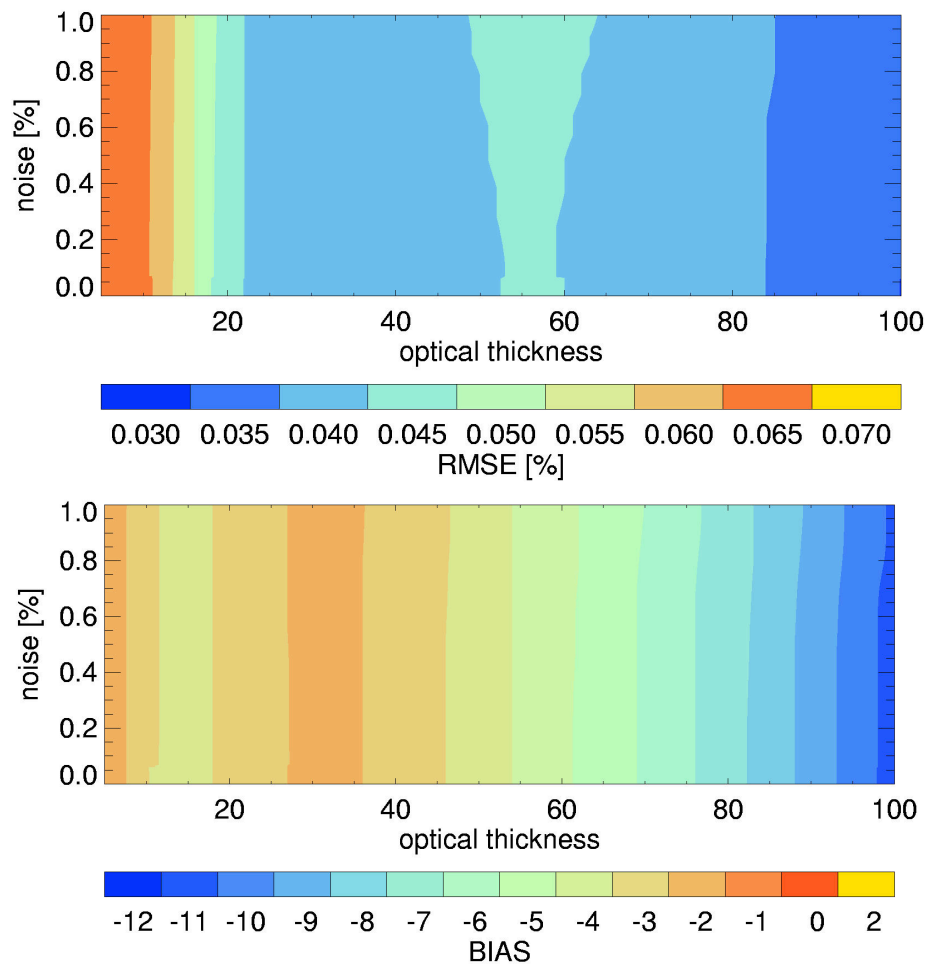

Figure 12: Sensitivity of the cloud optical thickness retrieval to cloud optical thickness and instrumental noise. Root mean square error RMSE (upper graph) and BIAS (lower graph).

3.3.3 Cloud albedo

3.3.3.1 Sensitivity to cloud optical thickness and cloud top height

The sensitivity of the cloud albedo retrieval to cloud optical thickness and cloud top height is shown in Figure 13. For higher optical thickness and cloud top height the RMSE of the cloud albedo retrieval decreases. In most of the cases the RMSE is below 0.04%. The BIAS is in the same range.
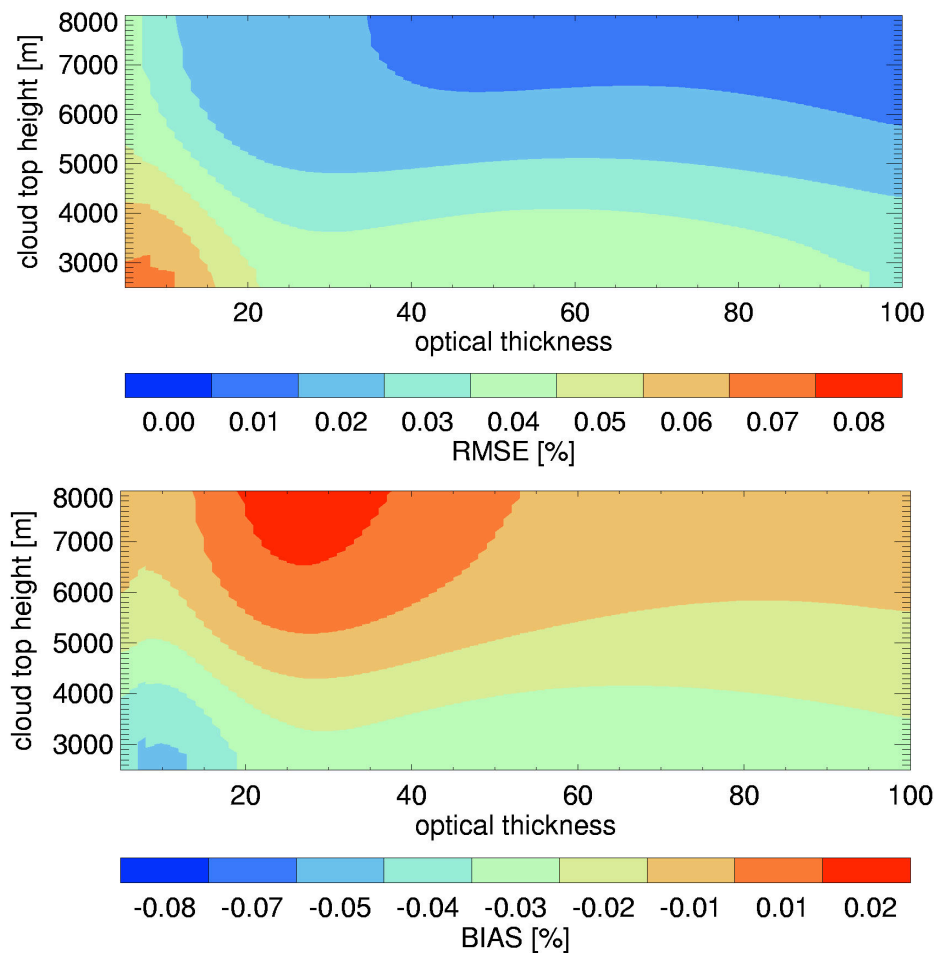

Figure 13: *Sensitivity of the cloud albedo retrieval to cloud optical thickness and cloud top height. Root mean square error RMSE (upper graph) and BIAS (lower graph).*

3.3.3.2 Sensitivity to cloud optical thickness and surface albedo

The sensitivity of the cloud albedo retrieval to cloud optical thickness and surface albedo is shown in Figure 14. The root mean square error (upper graph) is lowest for high cloud optical thickness and mean surface albedo values between 20 and 60 %. For most of the measuring conditions the RMSE is below 0.03 %. The BIAS (lower graph) is between –0.01 and 0.01%.
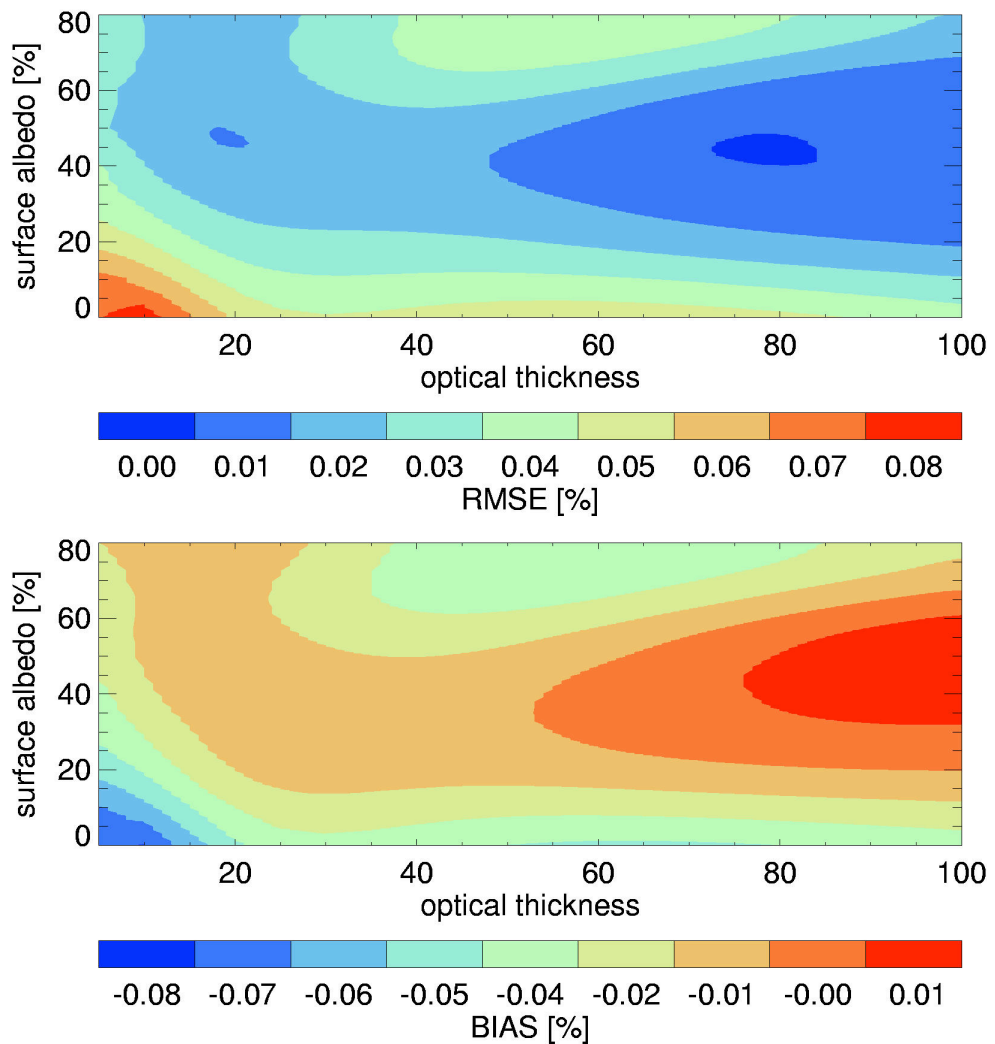

Figure 14: *Sensitivity of the cloud albedo retrieval to cloud optical thickness and surface albedo. Root mean square error RMSE (upper graph) and BIAS (lower graph).*

3.3.3.3 Sensitivity to cloud optical thickness and instrumental noise

The sensitivity of the cloud albedo retrieval to cloud optical thickness and instrumental noise is shown in Figure 15. The root mean square error is in most of the considered cases below is 0.04% (upper graph). The negative BIAS is below 0.03% (lower graph).
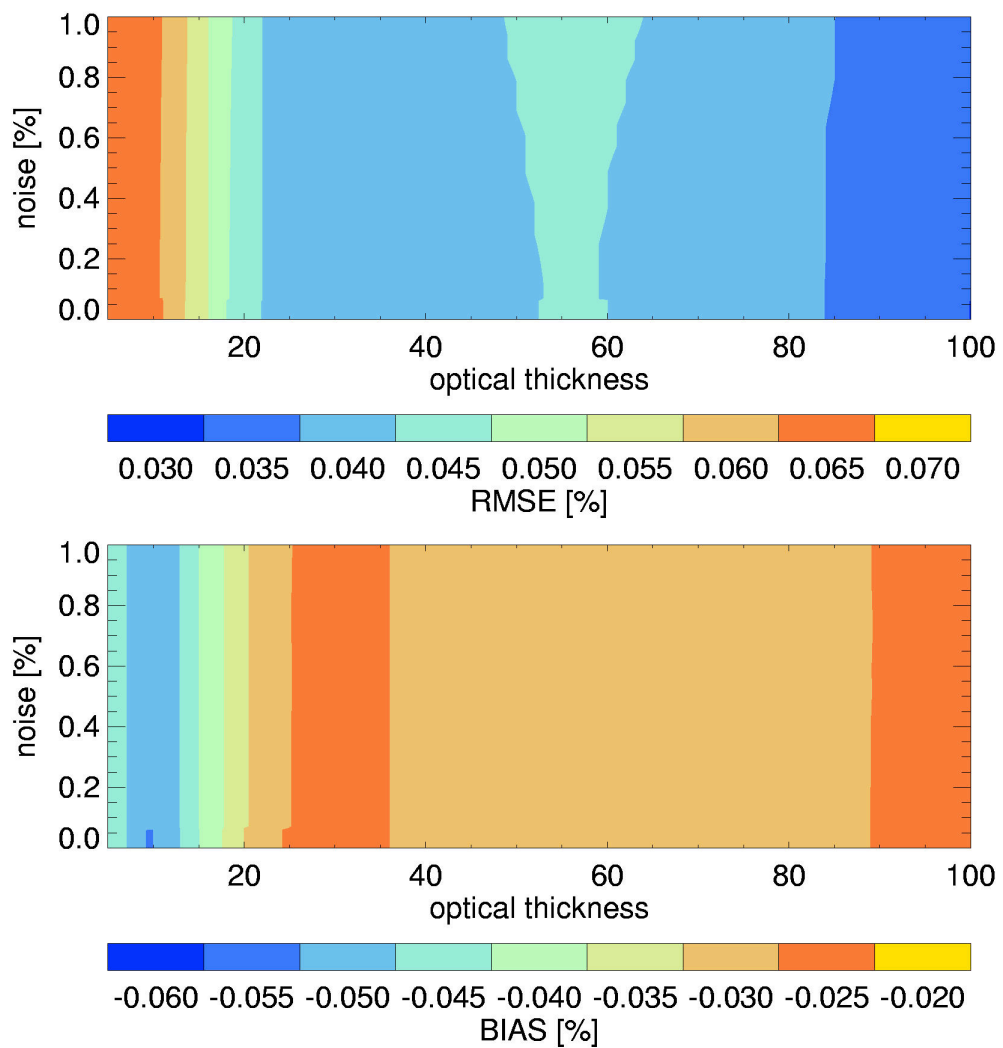

Figure 15: Sensitivity of the cloud albedo retrieval to cloud optical thickness and instrumental noise. Root mean square error RMSE (upper graph) and BIAS (lower graph).

4 Assumptions and Limitations

The algorithm is based on radiative transfer calculations for which a plan parallel atmosphere is assumed. For low sun elevations and high observation angles, the assumption of a plan parallel atmosphere is less fulfilled. Except for the Monte-Carlo method, there are no 3-dim radiative transfer codes available, which could describe the shape of the clouds more realistically. Nevertheless such radiative transfer codes have also significant limitations to describe 3-dim clouds adequately.

Effects from non-horizontal homogenous clouds cannot be treated with the MOMO model, but the influence of vertical distribution of cloud appearance are described. The environment effects of neighbouring pixels cannot be treated with the MOMO model.

5 References

Arking, A., 1990: The radiative effects of clouds and their impact on climate. Technical Report WCRP-52, WMO/TD-No. 399, International Council of Scientific Unions and World Meteorological Organisation.

Bakan *et al.* , 1998: CIVEX Field Phase Report. Max-Planck-Institut für Meteorologie, Hamburg.

Bennartz, R., and J. Fischer, 2000: A modified k-distribution approach applied to narrow-band water vapour and oxygen absorption estimates in the near infrared. J. Quant. Spectrosc. Radiat. Transfer, 66, 539–553.

Brenguier, J.-L., H. Pawlowska, L. Schüller, R. Preusker, J. Fischer and Y. Fouquart, 2000: Radiative properties of boundary layer clouds: droplet effective radius versus droplet concentration. J. Atmos. Sci., 57, 803-821.

Chandraesekhar, S., 1950: *Radiative Transfer*, Oxford University Press.

Charlson, R. J., J. E. Lovelock, M. O. Andrae, and S. G. Warren, 1987: Oceanic phytoplankton, atmospheric sulphur, cloud albedo and climate, *Nature*, **326**, 655-661.

Curran, R. J. and M. L. C. Wu, 1982: Skylab near-infrared observations of clouds indicated supercooled liquid water droplets. *J. Atmos. Sci.*, **39**, 635-647.

Feigelson, E. M., 1984: Radiation in a cloudy atmosphere, D. Riedel Publishing Company, Dordrecht

Fell, F., and J. Fischer, 2001: Numerical simulation of the light field in the atmosphere–ocean systemusing thematrix-operator method. J. Quant. Spectrosc. Radiat. Transfer, 3, 351–388

Fischer, J., and H. Grassl, 1984: Radiative transfer in an atmosphere–ocean system: An azimuthally dependent matrix-operator approach. Appl. Opt., 23, 1032–1039.

Fischer, J., and H. Graßl 1991: Detection of Cloud-Top Height from Backscattered Radiances within the Oxygen A-Band - Part 1: Theoretical Study.- *J. Appl Met.*, **30**, 1245-1259

Fischer, J., W. Cordes, A. Schmitz-Peiffer, W. Renger and P. Mörl, 1991: Detection of Cloud-Top Height from Backscattered Radiances within the Oxygen A-Band Part 2: Measurements. *J. Appl Met.*, **30**, 1260-1267.

Fischer, J. and M. Kollewe, 1994: Study of cloud top height determination using a coarse spatial resolution imaging spectrometer.- Final Report, ESA-ESTEC study, RFQ/3- 7241/91/NL/ BI.

Hansen, J. E. and L. D. Travis, 1974: Light scattering in planetary atmospheres. *Space Sci. Rev..*, **16**, 527-610

Hale, G. M. and M. R. Querry, 1973: Optical constants of water in the 200nm to 200μm wavelength region. *Appl. Opt.*, **12**, 555-563.

Heinemann, Th. and B. Gentili, 1995: Comparison between Radiances calculated by the Villefranche Monte-Carlo Model and the Berlin Matrix-Operator-Model (MOMO), WP 5000 Radiative Transfer Simulations Preliminary Report.

Lee, J., R.C. Wegner, S.K. Sengputa, and R.M. Welch, 1990: A neural network approach to cloud classification.- *IEEE Transactions on Geoscience and Remote Sensing*, **28** (5), 846-855.

Lindstrot, R., R. Preusker, T. Ruhtz, B. Heese, M. Wiegner, C. Lindemann, and J. Fischer, 2006: Validation of MERIS Cloud-Top Pressure Using Airborne Lidar Measurements. *J. Appl. Meteor. Climatol.,* **45**, 1612–1621.

Lindstrot, R, Preusker, R. and Fischer, J., 2010: The empirical correction of stray light in the MERIS oxygen A band channel, *J. Atmos. Oceanic Technol.,* **27 (7)**, 1185-1194.

Merheim-Kealy, P., J. P. Huot, and S. Delwart, 1999: The MERIS ground segment. Int. J. Remote Sens., 20, 1703–1712.

Muller, J.-P., R. Preusker, J. Fischer, M. Zuhlke, C. Brockmann, and P. Regner, 2007: ALBEDOMAP: MERIS land surface albedo retrieval using data fusion with MODIS BRDF and its validation using contemporaneous EO and in situ data products. Proc. IGARSS Int. Geoscience and Remote Sensing Symp., Barcelona, Spain, Institute of Electrical and Electronics Engineers, 2404–2407.

Nakajima, T. and M. D. King, 1990: Determination of the optical thickness and effective particle radius of clouds from reflected solar radiation measurements. Part I: Theory, *J. Atmos. Sci.*, **47,** 1879-1892.

Ohring, G. and S. Adler, 1978: Some experiments with a zonally averaged climate model, J. *Atmos. Sci.*, **35**, 186-205.

Palmer, K. F. and D. Williams, 1974: Optical properties of water in the near infrared, *J. Opt. Soc. Amer.*, **64**, 1107-1110.

Preusker, R., and R. Lindstrot, 2009: Remote Sensing of Cloud-Top Pressure Using Moderately Resolved Measurements within the Oxygen A Band—A Sensitivity Study. *J. Appl. Meteor. Climatol.*, **48**, 1562–1574.

Pruppacher, H. R. 1980: Microstructure of atmospheric clouds and precipitation. *Clouds: Their Formation, Optical Properties adn Effects*, P. Hobbs and A. Deepack, Eds. 93-185

Raes, F., 1996: Aspects of tropospheric aerosols: Questions and ACE 2, Proc. 14th Int. Conf. Nucleation

Roeckner, E., U. Schlese, J. Biercamp and P. Loewe, 1987: Cloud optical depth feedbacks and climate modelling. *Nature*, **329**, 138-140.

Ramanathan, V., R. D. Cess, E. F. Harrison, P. Minnis, B. R. Barkstrom, E. Ahmad, D. Hartmann, 1989: Cloud radiative forcing and climate: Results from the Earth Radiation Budget Experiment. *Science*, **243**, 57-63.

Rossow, W. B., 1989: Measuring cloud properties from space: A review. *J. Climate*, **2**, 201-213.

Rossow, W. B. and A. A. Lacis, 1988: Global, seasonal cloud variations from satellite measurements. Part II: Cloud properties and radiative effects. *J. Climate*, **3**, 1204-1253.

Rothman, L.S., I.E. Gordon, A. Barbe, D.C. Benner, P.F. Bernath, M. Birk, V. Boudon, L.R. Brown, A. Campargue, J.-P. Champion, K. Chance, L.H. Coudert, V. Dana, V.M. Devi, S. Fally, J.-M. Flaud, R.R. Gamache, A. Goldman, D. Jacquemart, I. Kleiner, N. Lacome, W.J. Lafferty, J.-Y. Mandin, S.T. Massie, S.N. Mikhailenko, C.E. Miller, N. Moazzen-Ahmadi, O. Naumenko, A.V. Nikitin, J. Orphal, V.I. Perevalov, A. Perrin, A. Predoi-Cross, C.P. Rinsland, M. Rotger, M. Simecková, M.A.H. Smith, K. Sung, S.A. Tashkun, J. Tennyson, R.A. Toth, A.C. Vandaele, and J. Vander Auwera, 2009: The *HITRAN* 2008 molecular spectroscopic database, JQSRT, **110**, 533-572.

Santer, R., F. Zagolski, D. Ramon, J. Fischer and P. Dubuisson, 2005: Uncertainties in radiative transfer computations: consequences on the MERIS products over land. Int. J. Remote Sensing, 26, No. 20,

Schüller, L., J. Fischer, W. Armbruster and B. Bartsch, 1997: Calibration of high resolution remote sensing instruments in the visible and near infrared. *Adv. Space Res.*, **19**, 1325-1334.

Sellers, P.J., W. Meeson, J. Closs, J. Collatz, F. Corprew, D. Dazlich, F. G. Hall, Y. Kerr, R. Koster, S. Los, K. Mitchell, J. McManus, D. Meyers, K.-J. Sun, and P. Try, 1996: The ISLSCP Initiative I global datasets: Surface boundary conditions and atmospheric forcings for land-atmosphere studies. *Bull. Amer. Meteor. Soc.*, **77**, 1987-2005.

Stephens, G. L, 1978: Radiation profiles in extended water clouds II: Parameterization schemes, *J. Atmos. Sci.*, **35,** 2123-2132.

Taylor, V. R. and L. L. Stowe, 1984: Reflectance characteristics of uniform earth and cloud surfaces derived from NIMBUS-7 ERB. *J. Geo. Res.* ,**89**, 4987-4996

Toon, O. B. and J. B. Pollack, 1973: A global Average Model of Atmospheric Aerosols for Radiative Transfer Calculations, *J. Appl. Met*, **15**, 225-246

Twomey, S., 1977: The influence of pollution on the shortwave albedo of clouds. *J. Atmos. Sci.*, **34,** 1149-1152

Twomey, S. and K. J. Seton, 1980 Inferences of gross microphysical properties of clouds from spectral reflectance measurements. *J. Atmos. Sci.*, **37**, 1065-1069.

WCP-report No. 112, 1986: A preliminary cloudless Standard Atmosphere for Radiation Computation, WMO/TD-No. 24.

Wiscombe, W. J., 1980: Improved Mie scattering algorithm, *Appl. Opt.*, **19**, 15505-1515.